Journal of Inorganic and General Chemistry
ZAAC
Zeitschrift für anorganische und allgemeine Chemie

DOI: 10.1002/zaac.201900211

ARTICLE

Anti-Tumor Activity of Doxorubicin-loaded Boehmite Nanocontainers

Carmen Seidl,[a] Sara Simonato,[b] Eva Zittel,[a] Ute Schepers,*[a] and Claus Feldmann*[b]

Dedicated to Professor Martin Jansen on the Occasion of his 75th Birthday

Abstract. Doxorubicin-filled boehmite nanocontainers, DOX@γ-AlO(OH), with a mean diameter of 40 nm and a wall thickness of 10 nm are prepared via a microemulsion strategy and studied as drug carriers for cancer treatment. Nanocontainer structure and drug load are examined in detail based on different analytical tools. The DOX load is optimized on highest load at lowest side effects according to blood counts. Cell uptake, DOX-based fluorescence detection and systemic toxicity are evaluated based on in vitro and in vivo models. Toxicity and activity of the DOX@AlO(OH) nanocontainers are compared with non-filled AlO(OH) hollow spheres and free DOX as references and show promising results. An orthotopic breast cancer BALB/c mouse model validates the activity of DOX@AlO(OH) in vivo at lower side effects than for free DOX.

1 Introduction

Doxorubicin (DOX) is one of the most widely used chemotherapeutics to date and used for treatment of a range of tumors, including liver and breast carcinoma or AIDS-related Kaposi's sarcoma.[1] The liposome-encapsulated form of DOX (so-called Doxil), moreover, is an established clinical standard.[1,2] DOX has nevertheless certain disadvantages such as high systemic toxicity (e.g. cardiotoxicity, heart arrhytmia, neutropenia), low selectivity towards tumor cells and rapid degradation in the physiological environment before reaching the cancer cells.[3] To improve drug transport and to decrease biodegradability and systemic toxicity of DOX simultaneously, nanocontainer systems have already proven to be advantageous.[4] In this regard, SiO_2-based mesoporous nanocontainers,[5] iron oxide,[6] gold,[7] or polymer-based[8] nanocontainers were studied most widely. Most of these studies, however, are limited to in vitro experiments, and they often did not consider side effects. Especially, SiO_2 has been critically discussed since recently due to its potential long-term carcinogenic effects.[9]

* Prof. Dr. U. Schepers
E-Mail: ute.schepers@kit.edu
* Prof. Dr. C. Feldmann
E-Mail: claus.feldmann@kit.edu
[a] Institute of Toxicology and Genetics
Karlsruhe Institute of Technology (KIT)
Hermann-von-Helmholtz-Platz 1
76344 Eggenstein-Leopoldshafen, Germany
[b] Institute of Inorganic Chemistry
Karlsruhe Institute of Technology (KIT)
Engesserstraße 15
76131 Karlsruhe, Germany
Supporting information for this article is available on the WWW under **http://dx.doi.org/10.1002/zaac.201900211** or from the author.

Nanocontainers are typically characterized by diameters of 80 to 120 nm; in some cases even larger particles have been described.[4–8] The DOX concentration in the nanocontainers can be rather high and was reported with loads up to 2100 mg·g^{-1}.[10] In general, a high concentration of doxorubicin is intended in order to achieve high cytotoxic effects. In regard of uncontrolled release, biodegradation, systemic toxicity and side effects,[1,3,4] however, efficient transport and release of DOX are just as important. Hence, the DOX concentration should preferably be optimized on highest activity at lowest side effects. Side effects as well as metastatic activity, however, were barely addressed in the literature.

Often nanocontainers with mesoporous walls are used to allow a sufficient release of DOX after the nanocontainer having entered single tumor cells or solid tumors.[4–6,8] A key issue for these systems is how to "switch off" and "switch on" the mesopores in response to biological or external stimuli. Moreover, membrane permeability, cell uptake and tumor infiltration are often hampered for such particles that often exceed the nanoregime (i.e. diameter $>$ 100 nm), especially, if certain particle agglomeration occurs as well. In this regard, nanoparticles with a mean diameter of 50 ± 20 nm have been reported as optimal in terms of tumor infiltration.[11] To address the aforementioned issues-including DOX concentration and cytotoxicity, systemic toxicity and side effects, cell uptake and drug release, targeted delivery, colloidal stability of the nanocarriers in physiological media, etc.-chemical synthesis and materials composition often have become more and more complex, including multi-step synthesis and sophisticated multi-component structures.[12]

As an alternative concept, we here suggest doxorubicin-filled boehmite nanocontainers, DOX@γ-AlO(OH), for drug delivery and cancer treatment, which show promising anti-tumor and anti-metastatic activities in combination with low side effects.

2 Results and Discussion

2.1 Synthesis of DOX@AlO(OH) Nanocontainers

AlO(OH) hollow spheres as nanocontainers were prepared via a microemulsion approach similar to our previous studies (Figure 1a).[13] The essential aspect of the synthesis strategy is related to reactants that were added to the different phases of the water-in-oil-(w/o)-microemulsion system. Thus, Al(*sec*-$OC_4H_9)_3$ as a lipophilic starting material was added to the lipophilic dispersion phase, whereas H_2O as a hydrophilic starting material was part of the polar droplet phase. As both reactants Al(*sec*-$OC_4H_9)_3$ and H_2O only meet at the water-to-oil phase boundary of the microemulsion, hydrolysis of the alkoxide is restricted to this phase boundary and results in solid AlO(OH) spheres that–at the end of the reaction–encapsulate the water droplets (Figure 1a). According to electron microscopy and dynamic light scattering, the as-prepared AlO(OH) nanocontainers exhibit an outer diameter of 30–50 nm, a cavity size of 20–30 nm and a wall thickness of 8–12 nm (Figure 1b–d and Figure S1, Supporting Information). High resolution images verify the thickness and crystallinity of the sphere wall with lattice distances of 3.2 Å (γ-AlO(OH)/boehmite: d(120) with 3.16 Å,[14] Figure 1b). Previous investigations have addressed the purity, crystallinity and specific surface area of the as-prepared AlO(OH) nanocontainers in detail.[13]

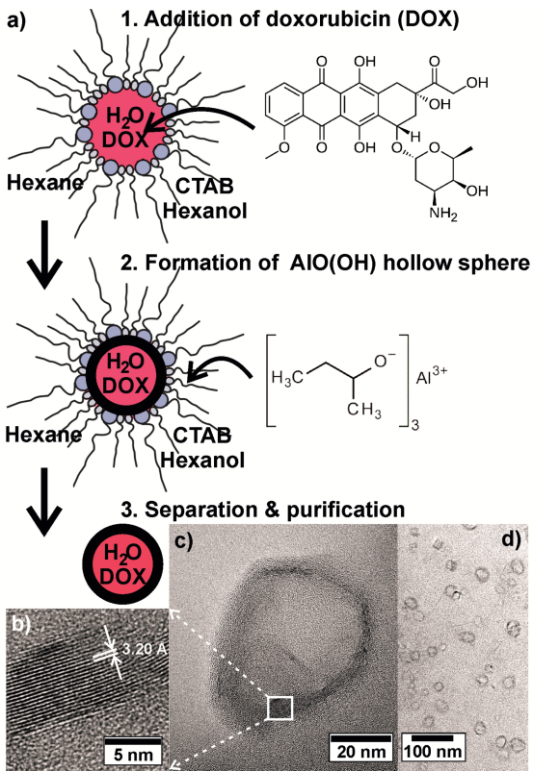

Figure 1. Synthesis of doxorubicin-filled boehmite nanocontainers (DOX@γ-AlO(OH)): (a) Scheme illustrating hollow sphere formation and DOX encapsulation; (b–d) size and structure according to transmission electron microscopy with: (b) high-resolution image of sphere wall, (c) high-resolution image of single hollow sphere, (d) overview image of hollow spheres.

Encapsulation of pharmaceuticals such as DOX inside the AlO(OH) nanocontainers is straightforward: hydrophilic drugs can be directly dissolved in aqueous droplets of the microemulsion. After sphere wall formation, the DOX-containing water droplet is encapsulated by AlO(OH) (Figure 1). In the as-prepared suspensions the hollow nanospheres are dense and do not show leakages or uncontrolled release, which was previously shown for several examples (e.g. release of rhodamine from AlO(OH) hollow nanospheres, release of thiourea from ZnO hollow nanospheres, release of isoniacid from Fe_2O_3 hollow nanospheres).[13,15] Following this strategy, doxorubicin (20 mg) was encapsulated in AlO(OH) hollow spheres (1 g). Successful DOX incorporation can be qualitatively detected based on the strong orange-red color of DOX@AlO(OH), whereas non-filled AlO(OH) hollow spheres are colorless (Figure 2a). Furthermore, the presence of DOX was proven by optical spectroscopy (UV/Vis, Figure 2b) and Fourier-transform infrared spectroscopy (FT-IR, Figure 2c and Supporting Information). Both show the characteristic absorption of DOX for DOX@AlO(OH), which is similar to pure DOX (Figure 2). Certain shifts of the respective absorptions between nanocontainers and free DOX can be ascribed to the interaction of DOX with the AlO(OH) sphere wall. Finally, the DOX concentration in the nanocontainers was determined based on optical spectra and by quantification via the Kubelka-Munk approach (Figure S2 and Table S2, Supporting Information), resulting in 22 mg DOX per 1 g of nanocontainers, which-

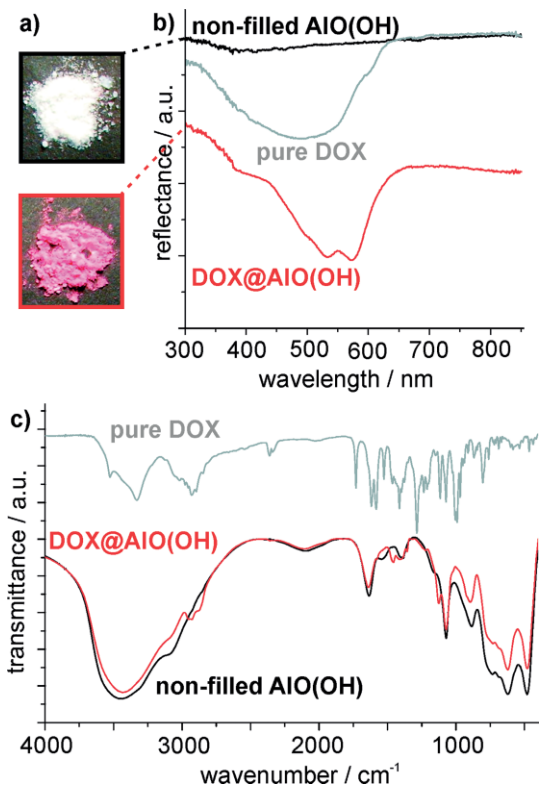

Figure 2. Presence of DOX in DOX@AlO(OH) nanocontainers: (a) Photos of powder samples; (b) UV/Vis spectra; (c) FT-IR spectra (non-filled AlO(OH) hollow spheres and pure DOX as references) (quantification of DOX content: Table S1, Figure S2, Supporting Information).

within the significance of the method-is in good accordance with the DOX amount introduced as a starting material.

The synthesis of the DOX@AlO(OH) nanocontainers was adjusted to meet the demands of the biomedical context:[13,15] after purification the DOX@AlO(OH) nanocontainers (75 $\mu g \cdot mL^{-1}$) were redispersed in aqueous dextran (4 $mg \cdot mL^{-1}$). Dextran coatings were often applied in the case of iron oxide nanoparticles,[16] which can be considered to be chemically similar to aluminum oxide. Dextran-coated DOX@AlO(OH) nanocontainers indeed showed an improved membrane penetration and cell uptake in comparison to non-coated nanocontainers. Additional aspects, such as the size, agglomeration, surface charge or type of cell, are of course also relevant.[17] With a final DOX concentration of 1.5 $\mu g \cdot mL^{-1}$, the applied concentration is at the lowest range of DOX concentrations used in other studies,[1–3,18] which is not necessarily disadvantagous if sufficient activity is combined with low side effects.

2.2 In vitro Studies

To investigate cell uptake and treatment related toxicity, human liver carcinoma cells (HepG2) and cervical cancer cells (HeLa) were incubated with DOX@AlO(OH) nanocontainers during cultivation. First, confocal laser scanning microscopy (CLSM) was used to analyze the biocompatibility of DOX@AlO(OH) qualitatively. DOX@AlO(OH)-treated HepG2 and HeLa cells do not show striking aberrations in morphology, and proliferation seems unimpaired within the investigated time frame of 24 hours (Figure 3; Figure S3a, Supporting Information). Based on the intense red fluorescence of doxorubicin (λ_{em} = 590 nm, λ_{exc} = 488 nm, argon laser),[19] CLSM can also be used to monitor the uptake of DOX@AlO(OH) into cells. The intracellular distribution of DOX@AlO(OH) is shown in Figure 3 (Figure S3a, Supporting Information). In comparison to cells treated with free DOX (Figure S3b, Supporting Information), DOX@AlO(OH)-treated cells display a more granular fluorescence, most likely caused by moderate clustering of the DOX@AlO(OH) nanocontainers. Some larger clusters might not be internalized due to steric hindrance but remain attached to the cell surface, whereas the majority of the nanocontainers is evenly distributed within perinuclear regions (Figure 3; Figure S3a, Supporting Information).

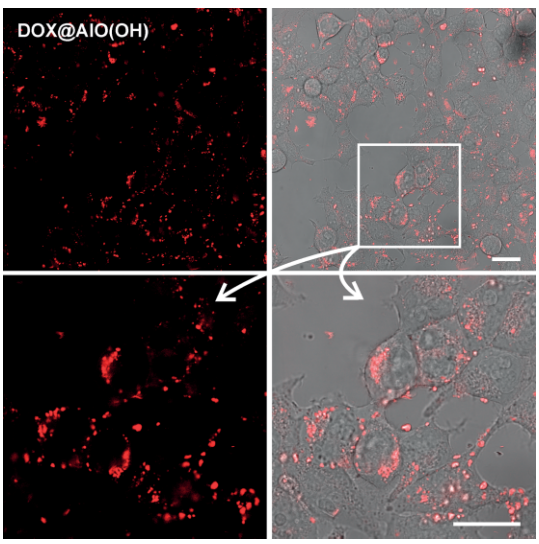

Figure 3. Cell uptake and fluorescence of DOX@AlO(OH) nanocontainers in human liver carcinoma cells (HepG2 cell line) according to CLSM images (argon laser with λ_{exc} = 488 nm, λ_{em} = 590 nm; scale bar is 25 µm).

Additionally, the cytotoxicity of DOX@AlO(OH) nanocontainers was quantified based on MTT (3-(4,5-dimethylthiazol-2-yl)-2,5-diphenyltetrazolium bromide) assays (Figure 4 and Figure S4, Supporting Information). For this purpose, HepG2 and HeLa cells were incubated for 72 h with different concentrations of DOX@AlO(OH) nanocontainers. Treating cells with DOX@AlO(OH) portions to obtain 0.25 to 1 µM of DOX highly impairs cell viability, which drops to around 20 %, generating an $LD_{50} < 0.25$ µM within the statistical error (Figure 4, Figure S4: red bars, Supporting Information). Obviously, DOX was successfully delivered into the cell and released from the dense AlO(OH) shell within the time frame of 72 hours, making the cells undergo apoptosis and necrosis. If free doxorubicin was administered in the same concentration range as a control, in contrast, cells are less affected and the LD_{50} is around 0.5 µM (Figure 4, Figure S4: brown bars, Supporting Information). For a further crucial control, cells were treated with non-filled AlO(OH) to exclude toxic effects from the delivery system itself (Figure 4, Figure S4: green bars, Supporting Information). Empty AlO(OH) hollow nanospheres proofed to be highly biocompatible with almost normal cell viability (90 %). Here, it needs to be noticed that the cell viability is even less affected than after treatment with massive AlO(OH) nanoparticles (Figure 4, Figure S4: light green bars, Supporting Information).

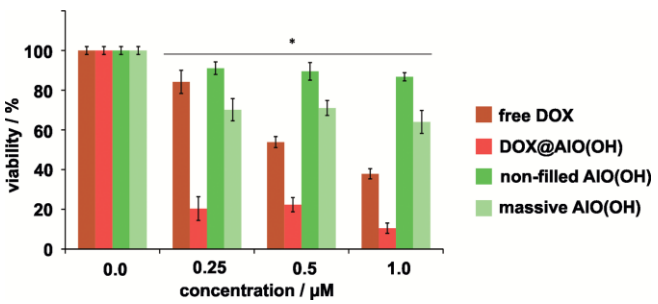

Figure 4. In vitro cytotoxicity of DOX@AlO(OH) nanocontainers in HepG2 cells using MTT assays with non-filled AlO(OH) nanocontainers, massive AlO(OH) nanoparticles and free DOX as controls (statistical error bars calculated from triplicates of n = 8; significance determined according to student's t-test with $p < 0.05$).

2.3 In vivo Studies

To validate the results gained in in vitro experiments, in vivo studies were performed to determine the effect of DOX@AlO(OH) on the progression of primary tumors and metastasis. This study was conducted in a breast cancer BALB/

c mouse model, where murine 4T1 breast-adenocarcinoma cells (1×10^6 cells per mL) were orthotopically implanted into the mammary fat pad of 8–12 weeks old female BALB/c-mice. In fact, this 4T1 cell line is an excellent system for investigating human breast cancer as it provides the opportunity to study the agent's impact not only on solid tumors but also on metastasis to organs affected in human breast cancer.

Eleven days after tumor induction, mice were intraperitoneally injected into the abdominal cavity with DOX@AlO(OH) nanocontainers (0.015 mg DOX/kg of body weight, in water). Injections of free DOX (2.5 mg·kg^{-1} of body weight, in PBS buffer) and physiological saline (DPBS) were used as positive and negative controls. It is to be noted that DOX is typically applied in doses of up to 20 mg·kg^{-1} of bodyweight in the literature.[20] Here, we use the lowest dose for anti-tumor treatment with free DOX that was found in the literature (2.5 mg·kg^{-1} of body weight). This concentration is nevertheless significantly higher than the DOX concentration available in the DOX@AlO(OH) nanocontainers (0.015 mg DOX per kg of body weight). The injections were performed trice a week for a total of seven doses (Figure 5). Throughout the experiment, body weight and volume of tumors were assessed (Figure 5; Figure S5, Supporting Information).

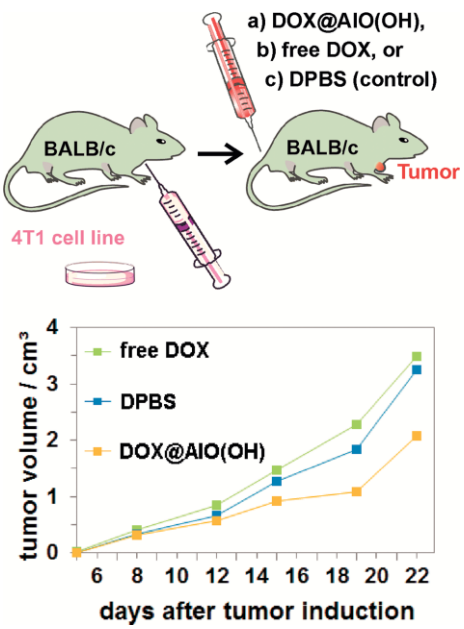

Figure 5. Scheme of animal treatments (1×10^6 4T1 cells inoculated into the mammary fat pad of BALB/c mice) and anti-tumor effect of DOX@AlO(OH) nanocontainers: tumor volumes as function of time for treatment with DOX@AlO(OH) nanocontainers (7×0.015 mg DOX/kg of bodyweight), free DOX (2.5 mg·kg^{-1} of bodyweight), and DPBS [each value represents the mean of $n = 8$ animals in the respective group; Figure S6 (Supporting Information) shows details with one graph per animal].

Mice did not show any abnormality or increased mortality during the study as indicated by their constant bodyweight (Figure S5, Supporting Information) and unaltered behavior. The tumors of mice increased in size from day 1 to 21 in all groups (Figure 5). However, tumor growth in DOX@AlO(OH)-treated mice is significantly impaired (Figure 5: yellow graph) as compared to the group treated with physiological saline (Figure 5: blue graph). After three weeks, primary tumors in mice treated with DOX@AlO(OH) nanocontainers are significantly smaller (volumes up to 3 cm^3) as compared to the tumors in the control groups treated with DPBS or free DOX (volumes up to 6 cm^3). Additionally, tumors of mice treated with DOX@AlO(OH) nanocontainers did not break up cortically as observed in both control groups. Interestingly, statistical spreading of tumor volumes is also more narrow within the DOX@AlO(OH) group (Figure S6, Supporting Information). The surprisingly high tumoricidal efficacy of the DOX@AlO(OH) nanocontainers can be ascribed to the well-accepted particle accumulation in tumor tissue due the enhanced permeability and retention (EPR) effect.[21] As the nanoparticles are accumulated in the tumor, slow dissolution of the AlO(OH) nanocontainers under physiological conditions results in a slow release of DOX directly into the tumor tissue. As a result, the maximum DOX concentration can be low and nevertheless guarantees for a significant effect. Moreover, advanced multistep syntheses and materials of high complexity of materials can be avoided.

In addition to the influence of DOX@AlO(OH) nanocontainers on primary tumors, DOX-related side effects and impacts on metastasis were studied as well. To this concern, blood was collected via cardiocentesis at the end of the study, namely just before sacrification of mice. Mice treated with DOX@filled AlO(OH) nanocontainers show a similar blood count to DPBS-treated control mice (Table S2, Supporting Information). In contrast, treatment with free DOX caused well-recognized side effects of chemotherapy, such as injury of liver, kidney and other organs (elevated levels of lipase and low levels of calcium, alkaline phosphatase and globulins; Table S2).[3,4,18,22] For free DOX, it can be concluded that side effects manifest already at low concentrations (2.5 mg·kg^{-1}, 4.6 µmol·kg^{-1} of bodyweight).

In contrast, DOX@AlO(OH) nanocontainers display high activity even in a low dose range of 0.015 mg DOX/kg of bodyweight without any significant side effects (according to blood counts, Table S2, Supporting Information). These findings can be ascribed to the rapid metabolic decomposition of free DOX in the body before reaching the cancer cells. In order to achieve similar activity in the tumor, significantly higher concentrations of free DOX (2.5 mg·kg^{-1} of body weight) are obviously necessary in comparison to DOX@AlO(OH) nanocontainers, which accumulate in the tumor tissue with their full DOX load (0.015 mg·kg^{-1} of body weight). Against the background of a severe tumor disease, the use of nanocontainers containing aluminum would most probably also be acceptable in view of the connection with Alzheimer's disease, which is often discussed but still not finally confirmed.[23]

Furthermore, the effect of DOX@AlO(OH) nanocontainers on metastatic spreading towards lymph nodes and lung was evaluated histologically. Hematoxylin/eosin stainings of 7 µm sections revealed that lungs of DPBS-treated mice contain multiple tumor nodules, harboring cells with abnormal morphology and polyploid nuclei (representative HE-stainings in Figure 6a). In contrast, metastatic foci were significantly re-

duced in organs of mice treated with DOX@AlO(OH) nanocontainers, indicating an anti-metastatic effect. For validation the volume of ipsilateral lymph nodes was assessed (Figure 6b and c). Here, the volume of lymph nodes draining the tumor is remarkably smaller in DOX@AlO(OH)-treated mice as compared to animals treated with DPBS, likewise substantiating the anti-metastatic potential of DOX@AlO(OH) nanocontainers.

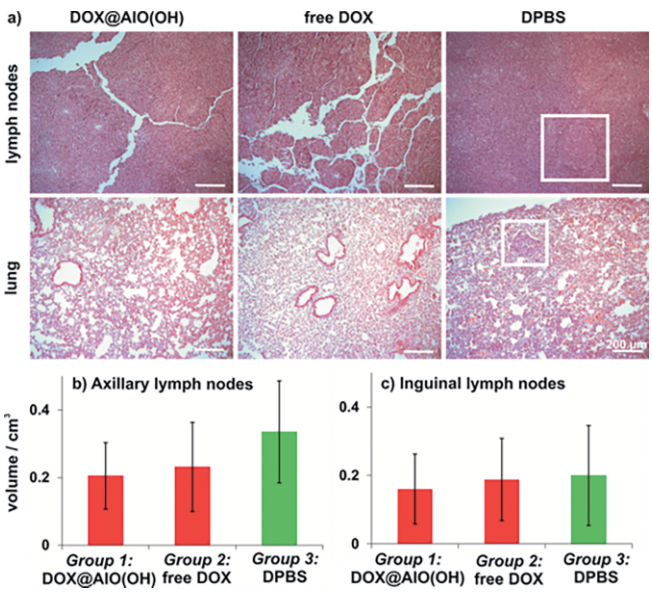

Figure 6. Anti-metastatic effect of DOX@AlO(OH) nanocontainers with: (a) Qualitative histological analysis of lymph nodes and lungs (haematoxylin- and eosin-stained histological sections) showing metastases of DPBS-treated mice in lymph nodes and lung (lung metastases also macroscopically visible-see frame), and quantification of the lymph-node metastasis by measuring the mean volumes of ipsilateral (b) axillary and (c) inguinal lymph nodes (n = 8; error bars indicate the statistical error).

3 Conclusions

Doxorubicin-filled boehmite nanocontainers [DOX@γ-AlO(OH)] are shown as drug-delivery system for cancer treatment. The AlO(OH) nanocontainers (mean diameter of 40 nm, wall thickness of 10 nm) are filled with DOX (20 mg·g^{-1}) via a straightforward microemulsion strategy. After dextran coating the nanocontainers are colloidally stable and show fast cell uptake. Cell uptake, fluorescence detection and systemic nanocontainer-related toxicity are evaluated based on human liver carcinoma cells (HepG2) and human cervical cancer cells (HeLa) as in vitro models. The comparison with non-filled AlO(OH) nanocontainers and free DOX proves the biocompatibility of the AlO(OH) nanocontainers and the encapsulation of DOX in DOX@AlO(OH).

In vivo studies based on an orthotopic breast cancer BALB/c mouse model prove the activity of DOX@AlO(OH) even at low concentration (0.015 mg DOX per kg of body weight) in comparison to free doxorubicin (2.5 mg DOX per kg of body weight). Very promising anti-tumor and anti-metastatic effects are observed. Notably, significant anti-tumor and anti-metastatic effects are observed at low DOX concentration and without observing typical DOX-related severe side effects. Due to the enhanced permeability and retention (EPR) effect, the DOX@AlO(OH) nanocontainers are accumulated in solid breast tumors without the need of advanced and complex materials, including the necessity of antibodies.

In sum, DOX@AlO(OH) nanocontainers show promising effects on the primary tumor and on metastasis as well as in combination with low side effects. These findings can be ascribed to the collection of the nanocontainers in the tumor tissue, which is driven by the EPR effect. Thereafter, the nanocontainers are slowly dissolved and can release all DOX into the tumor. With this strategy, on the one hand, unspecific biodegradation of DOX and side effects can be reduced. Due to the metabolic dissolution of the AlO(OH) nanocontainers, moreover, fast clearance from the body can be expected, which may help avoiding negative long-term effects (e.g. as recently reported for SiO_2). Detailed studies on, e.g., drug release, biodistribution and body clearance need to be performed next to explore dose-activity relations and to obtain suitable dosing schemes.

4 Experimental Section

4.1 Synthesis of DOX@AlO(OH) Nanocontainers

In general, the synthesis of nanoscale AlO(OH) nanocontainers follows our previously reported microemulsion approach.[13] The micellar system was established by *n*-hexane as the non-polar dispersant phase, a mixture of methanol and water (1 : 1) as the polar phase. Cetyltrimethylammonium bromide (CTAB) was used as the surfactant and *1*-hexanol as the co-surfactant (Figure 1). Doxorubicin (9.5 mg, doxorubicin hydrochloride, 98–102 %, Sigma–Aldrich) were dissolved in the methanol-water mixture and added as part of the polar phase of the microemulsion system. The presence of DOX is directly perceptible via its strong orange-red color. After establishing the microemulsion system and certain time of equilibration, Al(*sec*-$OC_4H_9)_3$ (246 mg, Aldrich, 97 %) was added to the hexane phase of the equilibrated, transparent orange *w/o*-microemulsion. In a period of 12 hours, the alkoxide was left to react at the water-to-oil phase boundary of the microemulsion system (Figure 1). The as-prepared DOX@AlO(OH) nanocontainers were collected via centrifugation. Thereafter, they were purified by sequential resuspension/centrifugation in/from 2-propanol and water. Finally, the DOX@AlO(OH) nanocontainers were redispersed in aqueous dextran (DOX@AlO(OH) with 0.075 mg/mL; dextran with 4 mg·mL^{-1}).

4.2 HepG2 and HeLa Cells

For confocal microscopy, 2 × 104 HepG2 (human liver carcinoma) or HeLa (human cervix carcinoma) cells were seeded into each well of a 8-well microslide Ibitreat from (IBIDI, Martinsried, Germany) and cultured in Dulbecco's modified Eagle's medium, high glucose, (DMEM, Invitrogen, Karlsruhe, Germany) supplemented with 10 % fetal calf serum (FCS, PAA) and 1 U·mL^{-1} penicillin/streptomycin at 37 °C, 5 % CO2. Confocal microscopy was performed with a Leica SP5 device (DMI6000).

MTT assays were performed to determine the cell viability (Figure 4). The yellow tetrazolium compound 3-(4,5-dimethylthiazol-2-yl)-2,5-di-

phenyltetrazolium bromide used in this assay was reduced to purple formazan by mitochondrial enzymes and quantified photometrically. As this reaction was limited to metabolically active cells, the amount of formazan is directly correlated with the cell viability. HepG2 and HeLa cells were seeded on 96-well plates at a density of 1×104 cells/well and cultivated at 37 °C and 5 % CO2. Cells were incubated with DOX@AlO(OH) nanocontainers in diverse concentrations for 1–3 d. Controls were treated with 5 µL Triton X-100. Afterwards, 15 µL of MTT solution (dye solution for MTT test, Promega) were added to each well and incubated for 1.5 h. The reaction was stopped by addition of 100 µL of lysis buffer. After 1.5 h, the absorbance of the converted dye was measured in a photometer (ultra microplate reader ELx808, BioTEK Instruments) at a wavelength of 595 nm.

4.3 Orthotopic Breast Cancer BALB/c Mouse Model

4T1 cells were maintained in DMEM medium supplemented with 10 % FCS and 1 % penicillin/streptomycin at 37 °C in a humidified incubator with 5 % CO_2. 1×10^6 cells in 100 µL of PBS were injected orthotopically into the mammary fat pad of 8–12 weeks old female BALB/c mice. Prior to injection, cells were tested for mycoplasma with the VenorGeM® Mycoplasma Detection Kit. 11 days after tumor induction, mice were randomized into four experimental groups (four mice per group). Mice were treated intraperitoneally with dextran-coated DOX@AlO(OH) nanocontainers (0.015 mg DOX/kg of bodyweight) trice a week for a total of seven doses. Control groups were treated with PBS or doxorubicin (2.5 $mg \cdot kg^{-1}$ of bodyweight) (Figure 5; Figure S6, Supporting Information). Animals were killed and an autopsy was performed when they became moribund or when tumors grew to the German legal limit.

The tumor growth was monitored by measuring the tumor diameters with calipers twice a week. The tumor volume was calculated using the formula $4/3 \cdot \pi \cdot a \cdot b \cdot c$ (ellipsoid). The treatment-related toxicity was determined by mouse weights weekly. Before the end of the study, 26 days after tumor induction, blood was collected via cardiocentesis (cf. Table S2, Supporting Information). Tumor, inguinal and auxiliary lymph nodes were dissected, weighed and measured in size (Figure 6). The lung was macroscopically examined for the occurrence of metastases. Lung, tumor and lymph nodes were fixed overnight in 3.7 % paraformaldehyd, embedded in paraffin and cut into sections for histological staining with hematoxylin and eosin. Animal procedures were approved by the regional government on animal experimentation in Germany: *35–9185.81/G-5/10*.

Supporting Information (see footnote on the first page of this article): More data related to the analytical tools, material characterization, the in vitro studies and in vivo studies can be found in the Supporting Information.

Acknowledgements

C.S and U.S. thank *Selma Huber* and *Manuela Sauer* for technical assistance. We also acknowledge the continuous support from the local animal facility at the ITG. S.S. and CF. are grateful to the German Research Society (DFG) for funding of equipment. The work was further supported by the Biointerfaces Program of the Helmholtz-Association (C.S. and U.S.).

Keywords: Nanocontainer; Doxorubicin; Tumor; Metastastasis; Side effects

References

[1] J. Ferlay, H. R. Shin, F. Bray, D. Forman, C. Mathers, D. M. Parkin, *Int. J. Cancer.* **2010**, *127*, 2893.
[2] Review: Y. Barenholz, *J. Contr. Relat.* **2012**, *160*, 117.
[3] Review: O. Tacar, P. Sriamornsak, C. R. Dass, *J. Pharm. Pharmacol.* **2013**, *65*, 157.
[4] Reviews: a) D. Rosenblum, N. Joshi, W. Tao, H. N. Karp, P. Dan, *Nature Commun.* **2018**, *9*, 1; b) T. Trantidou, M. Friddin, Y. Elani, N. J. Brooks, R. V. Law, H. M. Seddon, O. Ces, *ACS Nano* **2017**, *11*, 6549; c) D. Peer, J. M. Karp, S. Hong, O. C. Farokhzad, R. Margalit, R. Langer, *Nature Nanotechnol.* **2007**, *2*, 751.
[5] a) S. Wang, X. Liu, S. Chen, Z. Liu, X. Zhang, X. J. Liang, L. Li, *ACS Nano* **2019**, *13*, 274; b) K. Cheng, Y. Zhang, Y. Li, Z. Gao, F. Chen, K. Sun, P. An, C. Sun, Y. Jiang, B. Sun, *J. Mater. Chem. B* **2019**, *7*, 3291; c) L. Huang, G. Liu, F. Gao, Q. Cheng, B. Lu, H. Zheng, H. Xu, P. Xu, X. Zhang, X. Zeng, *J. Mater. Chem. B* **2018**, *6*, 4618; d) R. Jin, Z. Liu, Y. Bai, Y. Zhou, X. Chen, *ACS Omega.* **2018**, *3*, 4306; e) N. Li, D. Niu, Y. Jiang, C. Xu, S. Pan, H. He, J. Chen, L. Zhang, Y. Li, *Chem. Mater.* **2017**, *29*, 10377; f) M. Hei, J. Wang, K. Wang, W. Zhu, P. X. Ma, *J. Mater. Chem. B* **2017**, *5*, 9497; g) Y. You, L. He, B. Ma, T. Chen, *Adv. Funct. Mater.* **2017**, *27*,1.
[6] a) N. Pramanik, S. Ranganathan, S. Rao, K. Suneet, S. Jain, A. Rangarajan, S. Jhunjhunwala, *ACS Omega* **2019**, *4*, 9284; b) W. Chen, C. A. Cheng, J. I. Zink, *ACS Nano* **2019**, *13*, 1292; c) S. H. Hosseini, S. Alipour, N. Zohreh, *Langmuir* **2018**, *34*, 13735; d) M. Bellusci, P. Guglielmi, A. Masi, F. Padella, G. Singh, N. Yaacoub, D. Peddis, D. Secci, *Inorg. Chem.* **2018**, *57*, 1806; e) F. Benyettou, M. Alhashimi, M. O'Connor, R. Pasricha, J. Brandel, H. Traboulsi, J. Mazher, J. C. Olsen, A. Trabolsi, *ACS Appl. Mater. Interfaces* **2017**, *9*, 40006; f) Q. Zhang, L. Zhang, S. Li, X. Chen, M. Zhang, T. Wang, L. Li, C. Wang, *Chem. Eur. J.* **2017**, *23*, 17242.
[7] a) C. Peng, J. Xu, M. Yu, X. Ning, Y. Huang, B. Du, E. Hernandez, P. Kapur, J. T. Hsieh, J. Zheng, *Angew. Chem. Int. Ed.* **2019**, *58*, 8479; b) R. Deng, B. Ji, H. Yu, W. Bao, Z. Yang, Y. Yu, Y. Cui, Y. Du, M. Song, S. Liu, *Sci. Rep.* **2019**, *56*, 1; c) X. Zhang, Z. Xi, J. O. Machuki, J. Luo, D. Yang, J. Li, W. Cai, Y. Yang, L. Zhang, J. Tian, *ACS Nano* **2019**, *13*, 5306; d) Y. Wang, Q. Cui, X. Zhao, T. Qin, W. Wang, H. Sun, H. Zhu, H. Guo, H. Sun, *RSC Adv.* **2018**, *8*, 41454; e) S. Lee, G. Hwang, T. H. Kim, S. J. Kwon, J. U. Kim, K. Koh, B. Park, H. Hong, K. J. Yu, H. Chae, *ACS Nano* **2018**, *12*, 6756.
[8] a) Y. Li, S. Chen, X. Chang, F. He, R. Zhuo, *ACS Appl. Biomaterials* **2019**, *2*, 2271; b) C. Xu, D. Li, Z. Cao, M. Xiong, X. Yang, J. Wang, *Nano Lett.* **2019**, *19*, 2688; c) P. F. Cui, W. R. Zhuang, X. Hu, L. Xing, R. Y. Yu, J. B. Qiao, Y. J. He, F. Li, D. Ling, J. L. Jiang, *Chem. Commun.* **2018**, *54*, 8218; d) T. Senthilkumar, L. Zhou, Q. Gu, L. Liu, F. Lv, S. Wang, *Angew. Chem. Int. Ed.* **2018**, *57*, 13114; e) W. Wang, B. Wang, S. Liu, X. Shang, X. Yan, Z. Liu, X. Ma, X. Yu, *ACS Appl. Mater. Interfaces* **2017**, *9*, 15986; f) S. Xiang, H. J. Qian, Y. Chen, K. Zhang, Y. Shi, W. Liu, H. Sun, H. Sun, B. Yang, *Chem. Mater.* **2017**, *29*, 6536.
[9] F. Peng, M. I. Setyawati, J. K. Tee, X. Ding, J. Wang, M. E. Nga, H. K. Ho, D. T. Leong, *Nature Nanotechnol.* **2019**, *14*, 279.
[10] a) B. Wang, W. Meng, M. Bi, Y. Ni, Q. Cai, J. Wang, *Dalton Trans.* **2013**, *42*, 8918; b) J. You, G. Zhang, C. Li, *ACS Nano* **2010**, *4*, 1033.
[11] M. E. Davis, *Mater. Res. Soc. Bull.* **2012**, *37*, 828.
[12] Review: R. Freund, U. Laechelt, T. Gruber, B. Ruehle, S. Wuttke, *ACS Nano* **2018**, *12*, 2094.
[13] a) D. H. M. Buchold, C. Feldmann, *Nano Lett.* **2007**, *7*, 3489; b) S. Wolf, C. Feldmann, *Angew. Chem. Int. Ed.* **2016**, *55*, 15728.
[14] A. N. Christensen, M. S. Lehmann, P. Couvert, *Acta Chem. Scand. A* **1982**, *36*, 303.
[15] a) P. Leidinger, N. Dingenouts, R. Popescu, D. Gerthsen, C. Feldmann, *J. Mater. Chem.* **2012**, *22*, 14551; b) P. Leidinger, J. Treptow, K. Hagens, J. Eich, N. Zehethofer, D. Schwudke, W.

Öhlmann, H. Lünsdorf, O. Goldmann, U. E. Schaible, K. E. J. Dittmar, C. Feldmann, *Angew. Chem. Int. Ed.* **2015**, *54*, 12597.
[16] a) Y. Chao, P. P. Karmali, R. Mukthavaram, S. Kesari, V. L. Kouznetsova, I. F. Tsigelny, D. Simberg, *ACS Nano* **2013**, *7*, 4289; b) L. L. Ma, M. D. Feldman, J. M. Tam, A. S. Paranjape, K. K. Cheruku, T. A. Larson, J. O. Tam, D. R. Ingram, V. Paramita, J. W. Villard, *ACS Nano* **2009**, *3*, 2686.
[17] Review: C. Tassa, S. Y. Shaw, R. Weissleder, *Acc. Chem. Res.* **2011**, *44*, 842.
[18] a) K. Bourzac, *Nature* **2012**, *491*, S58; b) A. Asati, S. Santra, C. Kaittanis, H. M. Perez, *ACS Nano* **2010**, *4*, 5321.
[19] X. Dai, Z. Yue, M. E. Eccleston, J. Swartling, N. K. H. Slater, C. F. Kaminski, *Nanomedicine* **2008**, *4*, 49.
[20] a) O. Tacar, P. Sriamornsak, C. R. Dass, *J. Pharm. Pharmacol.* **2013**, *65*, 157; b) E. J. Kim, K. M. Lim, K. Y. Kim, O. N. Bae, J. Y. Noh, S. M. Chung, S. Shin, Y. P. Yun, J. H. Chung, *J. Thromb. Haemost.* **2009**, *7*, 1172; c) A. Gabizon, D. Tzemach, L. Mak, M. Bronstein, A. T. Horowitz, *J. Drug Target.* **2002**, *10*, 539.
[21] a) S. Taurin, K. Greish, *Cancer Metastas.* **2013**, *19*, 81; Review: b) H. Maeda, J. Wu, T. Sawa, Y. Matsumura, K. Hori, *J. Control. Release* **2000**, *65*, 271.
[22] M. J. Kim, H. K. Kim, *Acta Biol. Hung.* **2011**, *62*, 244.
[23] Review: K. P. Kepp, *Chem. Rev.* **2012**, *112*, 5193.

Received: August 30, 2019
Published Online: December 12, 2019

